1-1-2018

High performance MnO@C microcages with a hierarchical structure and tunable carbon shell for efficient and durable lithium storage

Chuanxin Hou
Shandong University, Shandong Normal University

Zhixin Tai
University of Wollongong, zt525@uowmail.edu.au

Lanling Zhao
Shandong University, lz083@uowmail.edu.au

Yanjie Zhai
Shandong University

Yue Hou
Shandong University

See next page for additional authors

High performance MnO@C microcages with a hierarchical structure and tunable carbon shell for efficient and durable lithium storage

Abstract

A MnO@C microcage with a multi-structure and tunable carbon shell was fabricated through a facile bio-inspired synthesis strategy for highly reversible Li storage. Micrometer-sized MnO unit aggregates were covered with a porous carbon shell outside with a thickness of about 0.2 μm, and a graphene-analogous carbon network inside the MnO@C microcages. The carbon shell could be tunable by a graphene-base shell. The unique double-carbon-coating structure of the MnO@C microcages enabled realizing the high Li-storage performance of the MnO particles with a micrometer size. The electrode containing the MnO@C microcages delivered a high reversible capacity of 1450.5 mA h g -1 after 270 cycles at a current density of 0.1 A g -1 , good rate capability, and outstanding cycling stability with a retention capacity of 805 mA h g -1 after 2000 cycles at a high current density of 1 A g -1 . Quantitative kinetic analysis indicated that around 40% of the charge storage came from the capacitive contribution of the microcage structure. It was found that the tunable graphene-base shell could enhance the Li-ion diffusion rate significantly, and enable a stable ultralong long life cycle performance and enhanced rate performance of the microcages.

Disciplines

Engineering | Physical Sciences and Mathematics

Publication Details

Hou, C., Tai, Z., Zhao, L., Zhai, Y., Hou, Y., Fan, Y., Dang, F., Wang, J. & Liu, H. (2018). High performance MnO@C microcages with a hierarchical structure and tunable carbon shell for efficient and durable lithium storage. Journal of Materials Chemistry A, 6 (20), 9723-9736.

Authors

Chuanxin Hou, Zhixin Tai, Lanling Zhao, Yanjie Zhai, Yue Hou, Yuqi Fan, Feng Dang, Jun Wang, and Hua-Kun Liu

High Performance MnO@C Microcages with a Hierarchical Structure and Tunable Carbon Shell for Efficient and Durable Lithium Storage

Chuanxin Hou,[1,2] Zhixin Tai,[3] Lanling Zhao,[4] Yanjie Zhai,[1] Yue Hou,[1] Yuqi Fan,[2] Feng Dang,[1] Jun Wang[1*] and Huakun Liu[3*]*

1. *Key Laboratory for Liquid-Solid Structural Evolution and Processing of Materials (Ministry of Education), Shandong University, Jinan 250061, P.R. China*
2. *Institute of Environment and Ecology, Shandong Normal University, Wenhuadong Rd 88, Lixia District, Ji'nan, 250014, China.*
3. *Institute* for *Superconducting and Electronic Materials, University of Wollongong, Wollongong, NSW 2522, Australia*
4. *School of Physics, Shandong University, Jinan, 250100, P.R. China*

E-mail: dangfeng@sdu.edu.cn

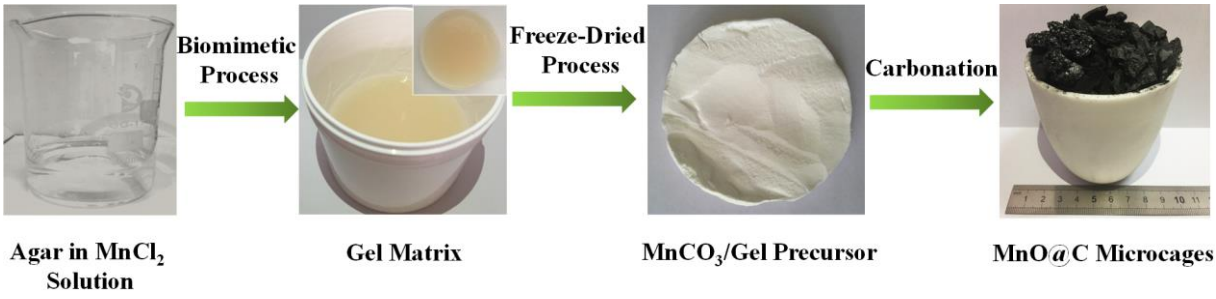

Figure S1. Schematic illustration of preparing MnO@C microcages.

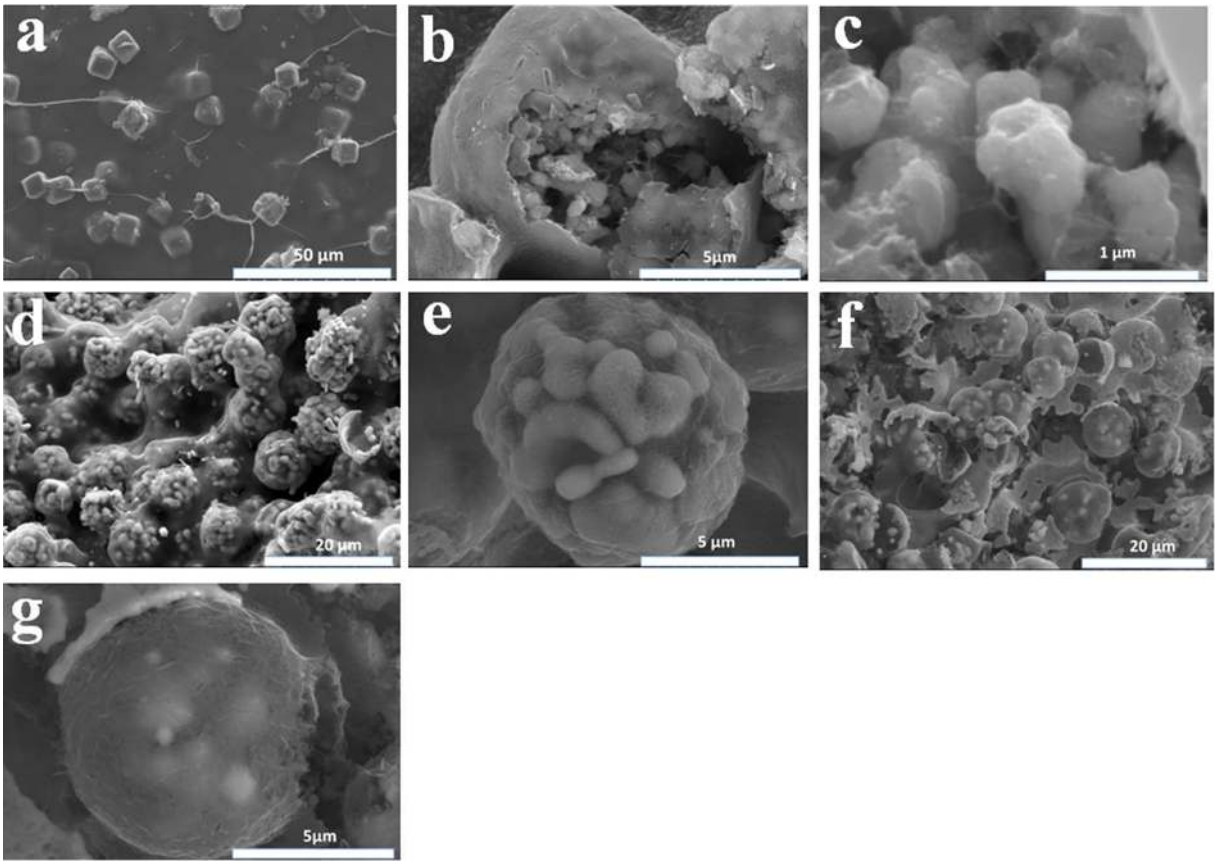

Figure S2. SEM images of $MnCO_3$ precursor particles (a)，MnO@C-700 (b,c), MnO@C-900 (d, e) and MnO@C-1100 (f, g).

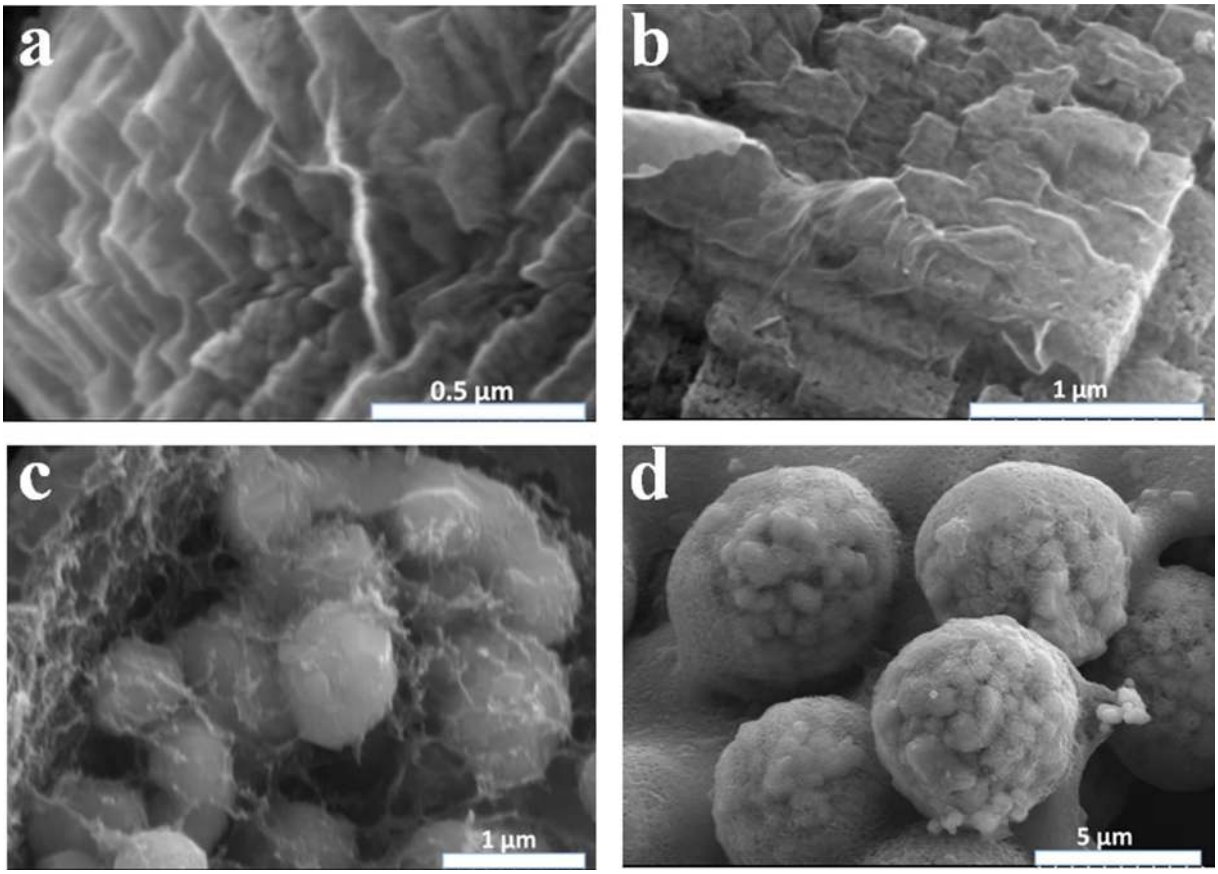

Figure S3. SEM image of the $MnCO_3$ processor contained graphene (0.9 wt%) (a, b), MnO@C-G9-700 contained graphene (c) and MnO@C-G12 microcage (d).

The formation mechanism and structure of biomimetic synthesized rhombohedral $MnCO_3$ particles have been studied and introduced by Oaki and Liu et al.[1-3] In the biomimetic process for the synthesis of $MnCO_3$, the rhombohedral $MnCO_3$ particles have a mesocrystal structure, in which small crystalline units grow in organic agar matrix and oriented aggregate into an organic-inorganic composite large particle. At the first stage, through the diffusion of CO_2 into the agar gel matrix, $MnCO_3$ nanocrystals grow and homogenously disperse in the organic matrix. Agar gel matrix will hinder the diffusion of nanocrystals. In the following stage, the nanocrystal will homoepitaxially aggregate rather than the classic atom-by-atom growth in the initial process due to the low initial adhesion force or energy, and the nanocrystal have sufficient time and freedom to align up epitaxially before irreversibly bounded together, finally forming the rhombohedral particles. The biological macromolecules play an important

role for the morphogenesis of $MnCO_3$ mesocrystals. Different macromolecules result into different morphologies of the $MnCO_3$ mesocrystals.

1. Y. Oaki, A. Kotachi, T. Miura, H. Imai, *Adv. Funct. Mater.*, **2006**, *16*,1633-1639.
2. T. Kokubu, Y. Oaki, E. Hosono, H. Imai, *Adv. Funct. Mater.*, **2011**, *21*, 3673-3680.
3. C. F. Liu, C. K. Zhang, H. Q. Song, G. P. Zhang, Y. G. Liu, X. H. Nan, G. Z. Cao, *Nano Energy*, **2016**, *22*, 290-300.

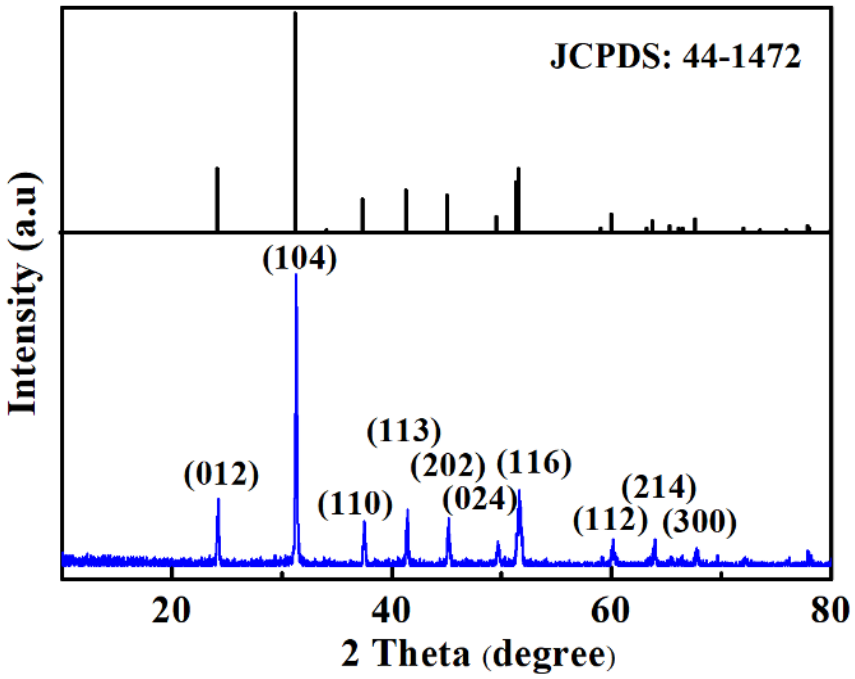

Figure S4. XRD pattern of $MnCO_3$/gel precursor.

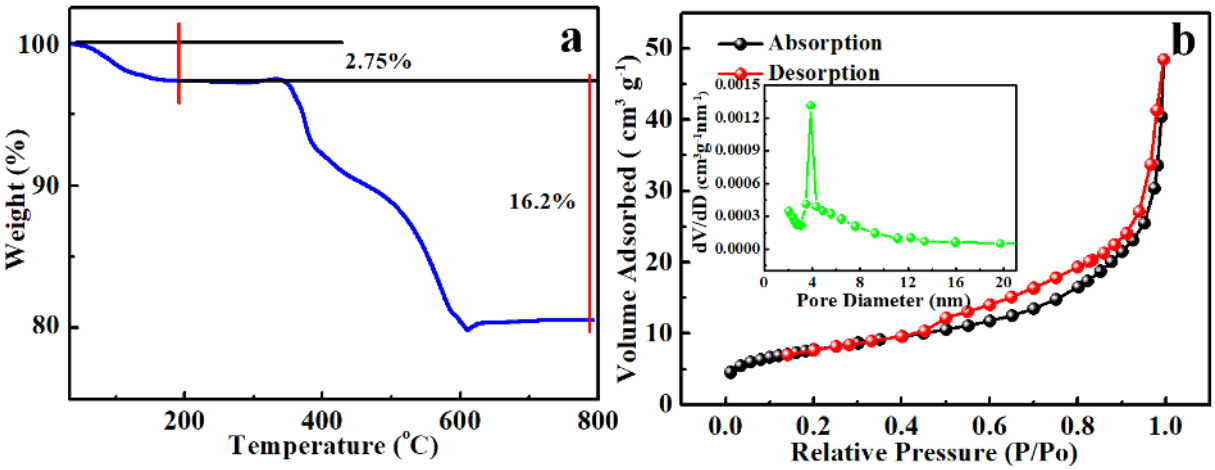

Figure S5. TGA curve of MnO@C-700 (a); nitrogen adsorption-desorption isotherm loop and pore size distribution curve calculated from desorption branch by the BJH model of MnO@C-700 (b).

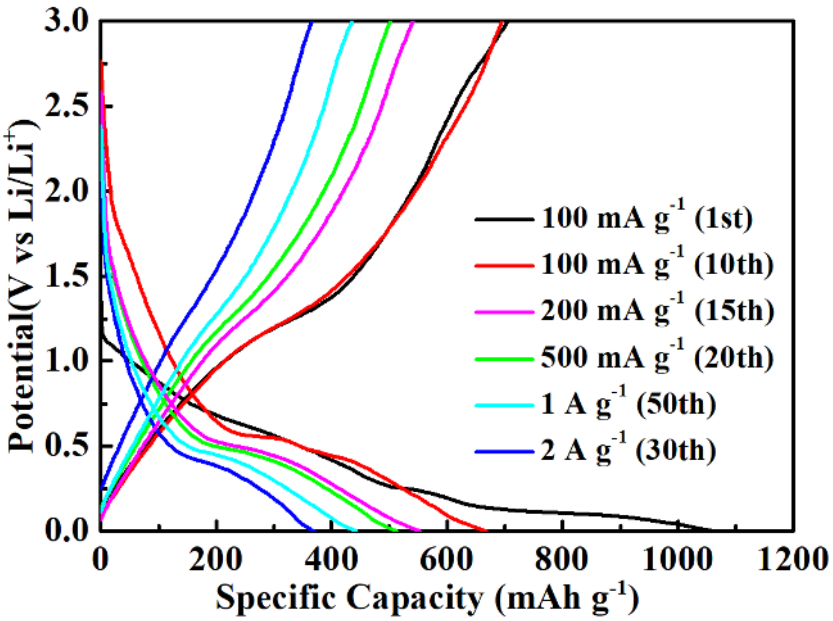

Figure S6. Charge-discharge profiles of MnO@C-700 electrodes at different current densities.

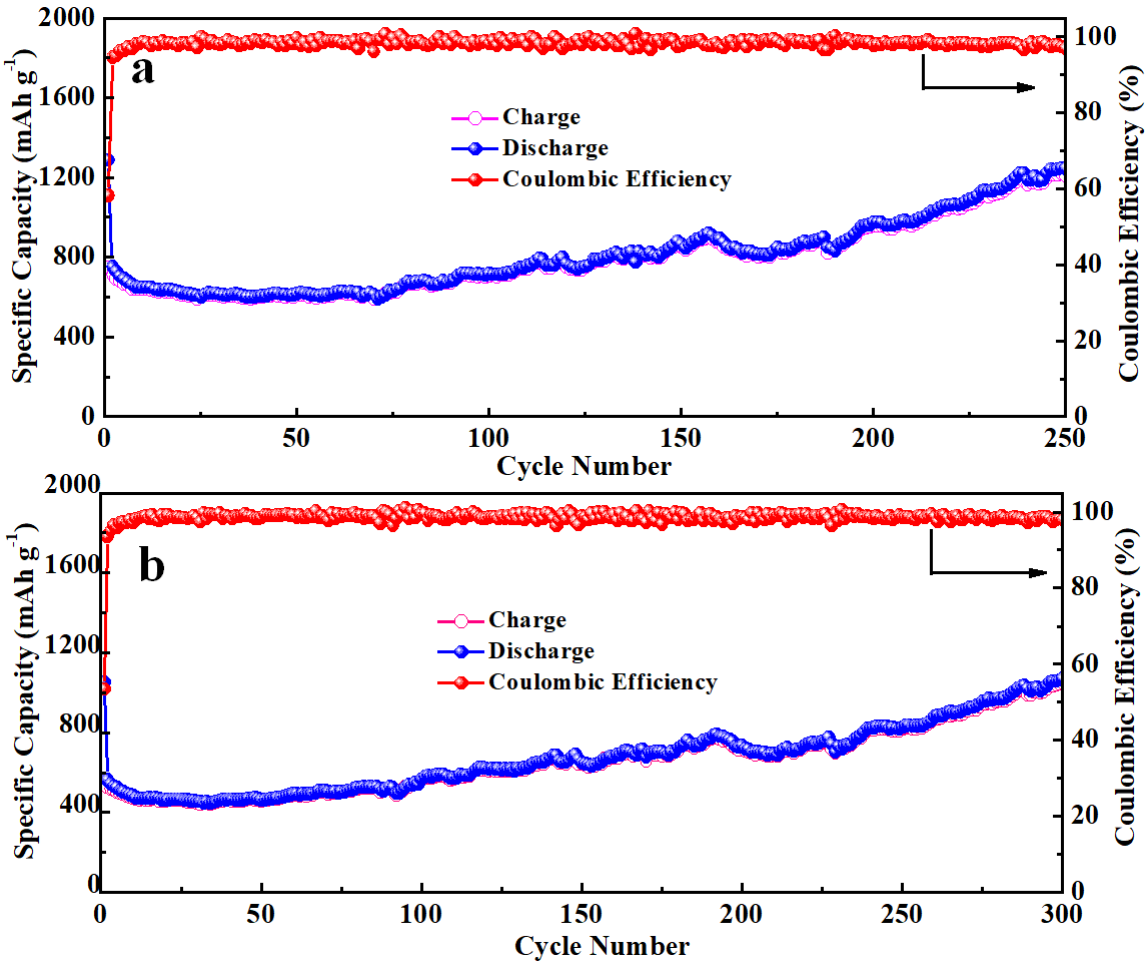

Figure S7. Cycling performance and coulombic efficiencies of MnO@C-900 (a) and MnO@C-1100 (b) electrodes at 0.1 A g^{-1}.

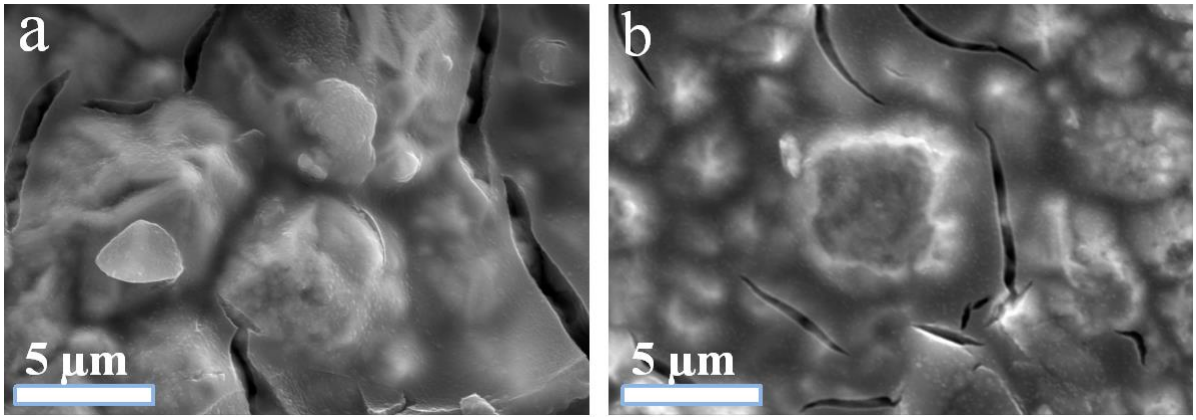

Figure S8. SEM images of MnO@C-900 (a) and MnO@C-1100 (b) electrodes after 250, 300 cycles, respectively, at 0.1 A g^{-1}.

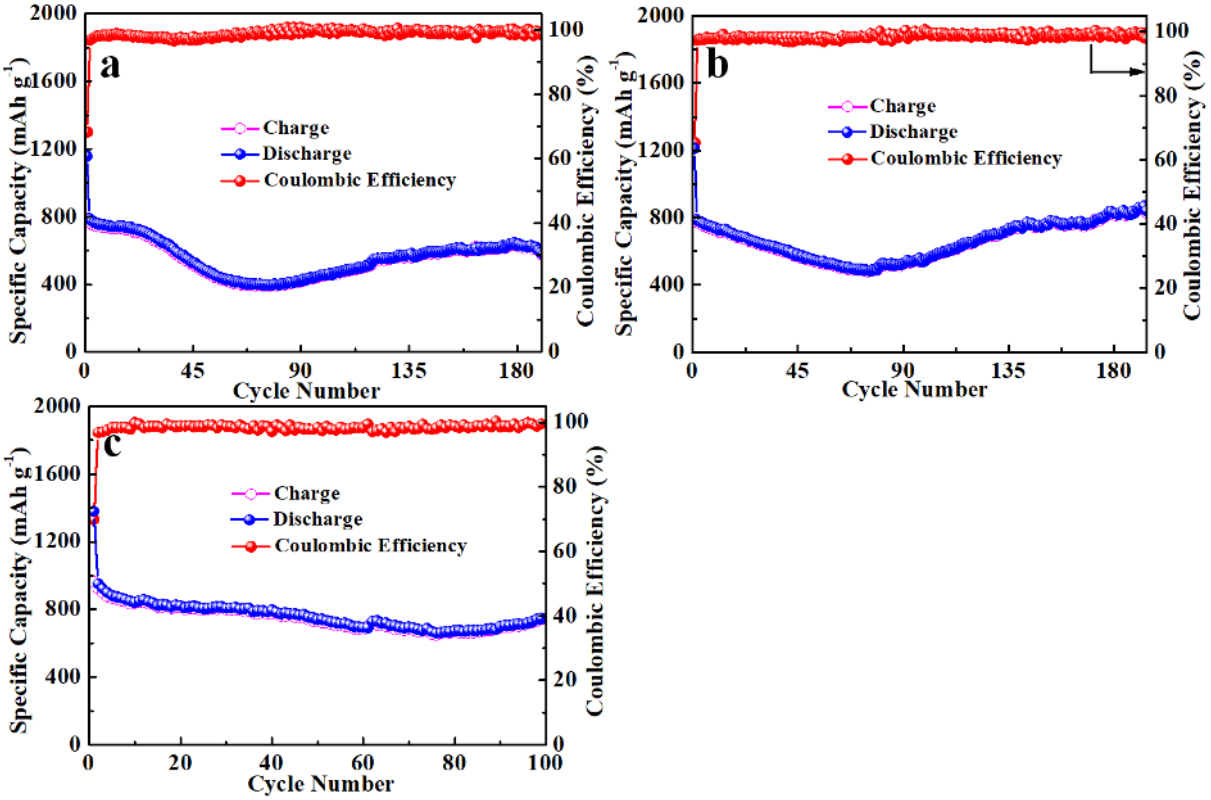

Figure S9. Cycling performance and coulombic efficiencies of MnO@C-G3-700 (a), MnO@C-G6-700 (b) and MnO@C-G12-700 electrodes at 0.1 A g^{-1}.

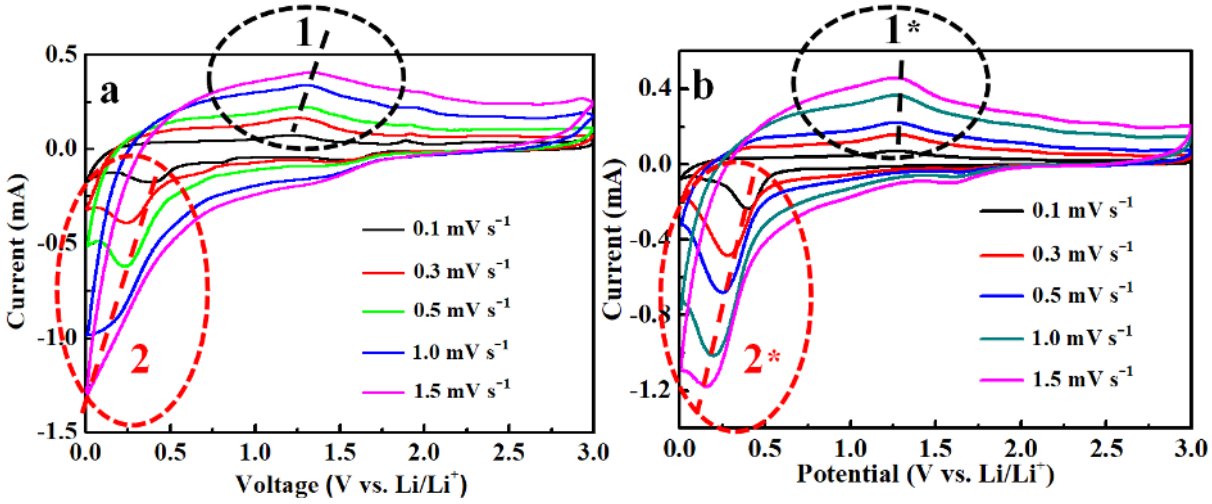

Figure S10. CV curves at differet scan rates from 0.1-1.5 mV s^{-1} of MnO@C-700 (a) and MnO@C-G9-700 (b) electrodes.

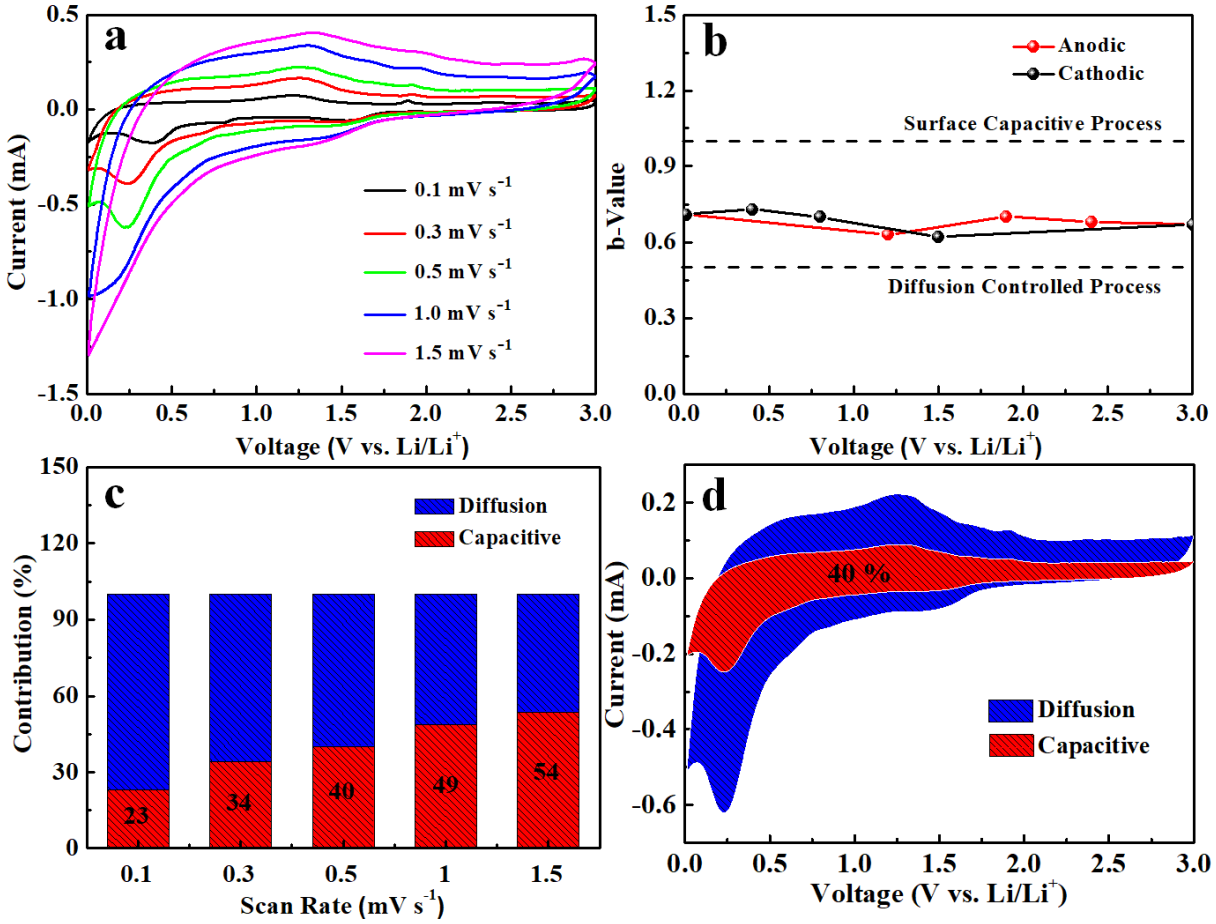

Figure S11. Kinetic analysis of the electrochemical behaviors of MnO@C-700 electrode: CV curves at different scan rates from 0.1-1.5 mV s^{-1} (a); b-values plotted against different battery potentials (b); the ratio of capacitive and diffusion contribution at different scan rates (c); the capacitive contribution to charge storage at scan rate of 0.5 mV s^{-1} (d).

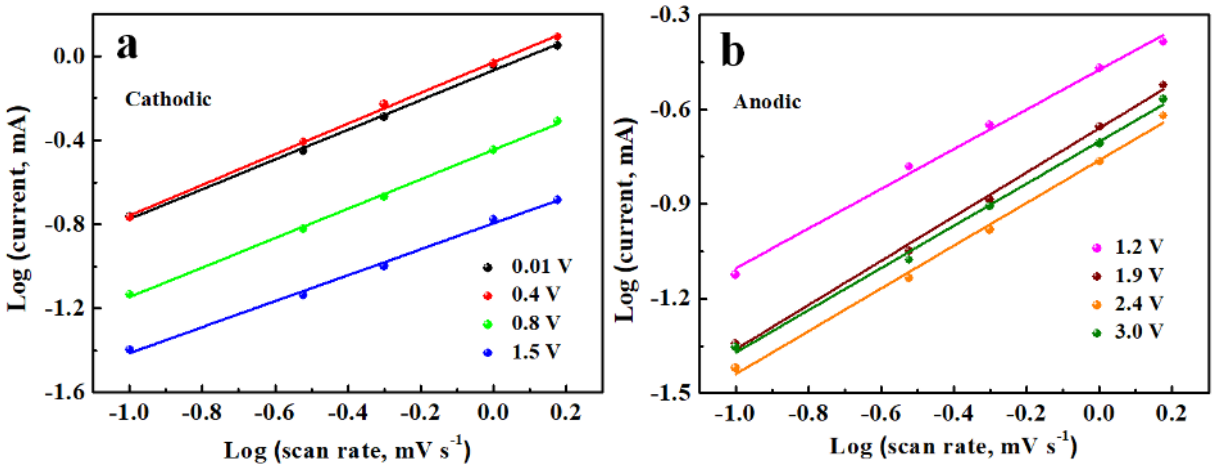

Figure S12. Current responses plotted against different scan rates of MnO@C-700 electrodes at different potentials for cathodic scans (a) and anodic scans (b).

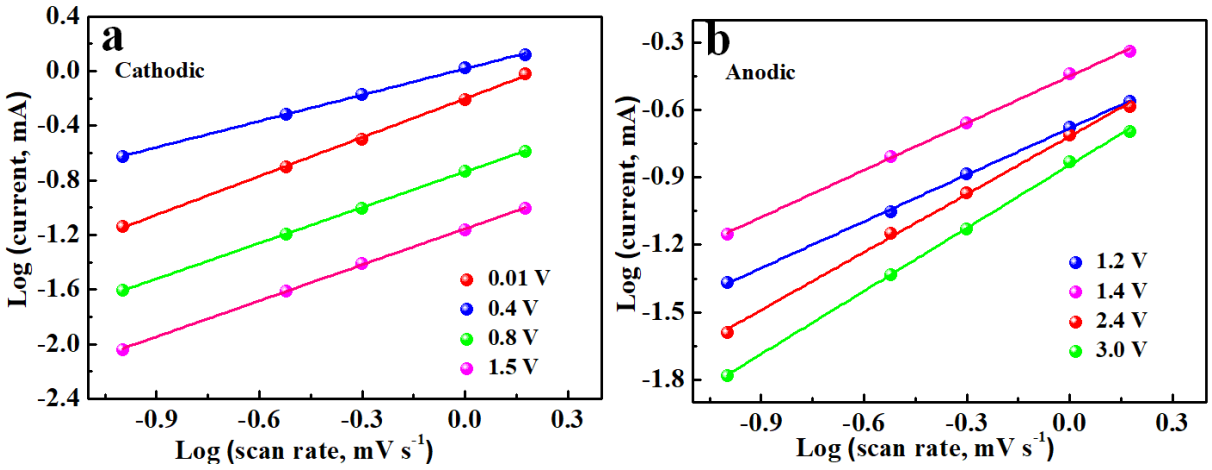

Figure S13. Current responses plotted against different scan rates of MnO@C-G9-700 electrodes at different potentials for cathodic scans (a) and anodic scans (b).